In-Flight Validation and Recovery of Water Surface Temperature With Landsat-5 Thermal Infrared Data Using an Automated High-Altitude Lake Validation Site at Lake Tahoe

Simon J. Hook, Gyanesh Chander, Julia A. Barsi, Ronald E. Alley, Ali Abtahi, Frank D. Palluconi, Brian L. Markham, *Member, IEEE*, Robert C. Richards, S. Geoffrey Schladow, and Dennis L. Helder, *Member, IEEE*

***Abstract*—The absolute radiometric accuracy of the thermal infrared band (B6) of the Thematic Mapper (TM) instrument on the Landsat-5 (L5) satellite was assessed over a period of approximately four years using data from the Lake Tahoe automated validation site (California–Nevada). The Lake Tahoe site was established in July 1999, and measurements of the skin and bulk temperature have been made approximately every 2 min from four permanently moored buoys since mid-1999. Assessment involved using a radiative transfer model to propagate surface skin temperature measurements made at the time of the L5 overpass to predict the at-sensor radiance. The predicted radiance was then convolved with the L5B6 system response function to obtain the predicted L5B6 radiance, which was then compared with the radiance measured by L5B6. Twenty-four cloud-free scenes acquired between 1999 and 2003 were used in the analysis with scene temperatures ranging between 4 °C and 22 °C. The results indicate L5B6 had a radiance bias of 2.5% (1.6 °C) in late 1999, which gradually decreased to 0.8% (0.5 °C) in mid-2002. Since that time, the bias has remained positive (predicted minus measured) and between 0.3% (0.2 °C) and 1.4% (0.9 °C). The cause for the cold bias (L5 radiances are lower than expected) is unresolved, but likely related to changes in instrument temperature associated with changes in instrument usage. The *in situ* data were then used to develop algorithms to recover the skin and bulk temperature of the water by regressing the L5B6 radiance and the National Center for Environmental Prediction (NCEP) total column water data to either the skin or bulk temperature. Use of the NCEP data provides an alternative approach to the split-window approach used with instruments that have two thermal infrared bands. The results indicate the surface skin and bulk temperature can be recovered with a standard error of 0.6 °C. This error is larger than errors obtained with other instruments due, in part, to the calibration bias. L5 provides the only long-duration high spatial resolution thermal infrared measurements of the land surface. If these data are to be used effectively in studies designed to monitor change, it is essential to continue to monitor instrument performance in-flight and develop quantitative algorithms for recovering surface temperature.**

***Index Terms*—Advanced Spaceborne Thermal Emission and Reflectance Radiometer (ASTER), emissivity, Lake Tahoe, Landsat, Landsat-5, Moderate Resolution Imaging Spectroradiometer (MODIS), temperature, thermal, validation.**

I. Introduction

THE Thematic Mapper (TM) instrument, flown on the Landsat-4 and Landsat-5 satellites, provides high spatial resolution visible through thermal infrared images of the land surface. These images constitute one of the few global high spatial resolution datasets suitable for monitoring land cover and land use change. The TM images the earth's surface in seven spectral bands. Six of the bands are located in the visible shortwave infrared part of the electromagnetic spectrum (0.5–2.5 μm) with an additional single band in the thermal infrared "emissive" part of the electromagnetic spectrum (10.4–12.5 μm). The reflective bands have spatial resolutions of 30 m, and the emissive band has a spatial resolution of 120 m for Landsat-4, -5, and -6. The Landsat-7 satellite carries the Enhanced Thematic Mapper plus (ETM+) instrument that includes the same reflective bands with 30-m spatial resolution as the Thematic Mapper and an additional panchromatic band with 15-m spatial resolution. Also, the spatial resolution of the emissive band on ETM+ has been improved from 120 to 60 m and made available in two gain states. Table I provides the key characteristics of the thermal infrared bands on Landsat-5 TM and Landsat-7 ETM+. While the six visible shortwave infrared bands have been extensively used in local and regional-scale studies, the thermal band has been less utilized, in part, due to concern over its calibration.

Landsat-5 was launched in March 1984 and continues to operate today, far beyond its expected lifetime. Since launch, periodic in-flight validation of the instrument has revealed that

Manuscript received February 16, 2004; revised September 22, 2004. This work was carried out in part at the Jet Propulsion Laboratory (JPL), California Institute of Technology (Caltech), under a contract with the National Aeronautics and Space Administration as part of the Earth Observing System Mission to Planet Earth Program. Reference herein to any specific commercial product, process, or service by trade names, trademark, manufacturer, or otherwise does not imply endorsement by the United States or the JPL, Caltech.

S. J. Hook, R. E. Alley, A. Abtahi, and F. D. Palluconi are with the Jet Propulsion Laboratory, California Institute of Technology, Pasadena, CA 91109 USA (e-mail: simon.j.hook@jpl.nasa.gov).

G. Chander is with the Science Application International Corporation, Earth Resources Observation System Data Center, U.S Geological Survey, Sioux Falls, SD 57198 USA (e-mail: gchander@usgs.gov).

J. A. Barsi is with the Science Systems and Applications, Incorporated, National Aeronautics and Space Administration Goddard Space Flight Center, Greenbelt, MD 20771 USA (e-mail: Julia.Barsi@gsfc.nasa.gov).

B. L. Markham is with the Landsat Project Science Office, National Aeronautics and Space Administration Goddard Space Flight Center, Greenbelt, MD 20771 USA (e-mail: Brian.L.Markham@nasa.gov).

R. C. Richards is with the Tahoe Research Group, Department of Environmental Science and Policy, University of California, Davis, CA 95616 USA.

S. G. Schladow is with the Department of Civil and Environmental Engineering, University of California, Davis, CA 95616 USA.

D. L. Helder is with the Electrical Engineering Department, South Dakota State University, Brookings, SD 57007 USA.

Digital Object Identifier 10.1109/TGRS.2004.839092

TABLE I
SPECIFICATIONS FOR THE THERMAL INFRARED BAND OF THE THEMATIC MAPPER INSTRUMENTS FLOWN ON LANDSAT-5 AND LANDSAT ETM+ (FROM [1])

Instrument	Full Width Half Maximum Bandpass (μm)	Spatial Resolution (m)	NEΔT (K at 280 K)	Radiometric Scaling Range (W / m2 sr μm)	Useful Temperature Range (K)
Landsat-5 TM	10.45-12.42	120	0.17-0.30	1.238-15.30	L1R: 180-350 L1G: 200 - 340
Landsat-7 ETM+	10.31-12.36	60	H: 0.22 L 0.28	H: 3.2 - 12.65 L: 0.0 - 17.04	H: 240 - 320 L: 130 - 350

the instrument performance has changed over the lifetime of the mission [1]. The calibration of L5B6 was first assessed by Schott and Volchok [25]. Their work indicated that the radiometric temperature reported by L5B6 was cooler than expected by 2 °C over a 26 °C temperature range. The results from this study were later revised by Schott [26] when the calibration was reported to within ±0.9 °C. The study by Schott and Volchok [25] provided a benchmark for the calibration of the thermal band but was hampered by the lack of well-developed radiative transfer codes (RTCs) for modeling atmospheric effects as well as suitable radiometers for accurately and precisely determining the surface skin temperature. More recently, O'Donnell *et al.* [21] reexamined the calibration of the L5B6 using historical data and determined a calibration difference of −2 to +1.5 K (L5 minus forward predicted ground data). The forward predicted ground data refer to the calculation of the at-sensor radiance using the ground data and a RTC. This study complements the work of Schott and O'Donnell providing accuracy assessments of L5B6 for 24 cloud-free scenes acquired between 1999 and 2003 over the Lake Tahoe automated validation site. A portion of the results presented in this paper was included in Barsi *et al.* [1], which, when used in conjunction with data from several other investigators, suggested a cold bias of 0.71 ± 0.2 °C at 300 K (radiances measured by L5B6 were lower than expected).

In addition to assessing the accuracy of L5B6, this work also provides algorithms for the recovery of water surface temperature from L5B6 data. Knowledge of the temperature distribution in water bodies is very valuable for understanding a variety of processes such as wind-induced upwelling events [11], [16]–[18] and surface water transport patterns [28], [29]. Obtaining *in situ* temperature data from boats is relatively straightforward and provides information on the vertical temperature distribution in a water body. However, such measurements provide little information on the horizontal distribution of temperature across a water body. By contrast, surface temperatures derived from satellite measurements provide information on the horizontal temperature distribution but no information on the vertical temperature distribution of the water body. As a result, temperature data obtained from both satellite data and *in situ* measurements are highly desirable to understand the thermal processes taking place in water bodies.

Typically, satellite instruments with at least two bands in the thermal infrared (7–13 μm) part of the infrared spectrum, such as the Advanced Very High Resolution Radiometer (AVHRR) or Along-Track Scanning Radiometers (ATSRs), have been used to recover the surface temperature of water (e.g., [15], [19], and [20]). These studies demonstrate that the sea surface temperature (SST) can be recovered to an accuracy of 0.3 °C. SST retrievals from AVHRR and ATSR involve applying a set of coefficients to the data from the infrared bands. These coefficients can be derived by regression of the satellite measurements to a series of *in situ* buoy temperature measurements (e.g., [20] and [31]) or to a series of modeled SSTs (e.g., [33]). Both these approaches have been validated by *in situ* measurements (e.g., [3], [8], and [24]). The two approaches produce different SSTs, since the buoy temperature measurements are made at depth, whereas the modeled SSTs utilize the radiometric temperature of the ocean skin. The sea surface skin temperature is typically 0.1 °C to 0.5 °C cooler than the bulk temperature, although the difference can vary considerably from this nominal range. The same approaches developed for deriving coefficients for SST with dual-band thermal infrared sensors can also be used to develop coefficients for retrieving lake surface temperature [10].

Since only one thermal infrared band is included on the TM, a different approach must be used to recover surface temperature with L5B6 data. A radiative-transfer-based solution is described by Barsi *et al.* [2], where a modeled profile is used to calculate the necessary correction (available online at http://tightrope.gsfc.nasa.gov/atm_corr/atm_corr.html). In this paper, an alternate approach is provided that uses the total column water vapor from a modeled profile for the time of the overpass.

II. SITE DESCRIPTION AND INSTRUMENTATION

Lake Tahoe is a large lake situated in a granite graben near the crest of the Sierra Nevada Mountains on the California–Nevada border, at 39 °N, 120 °W. The lake level is approximately 1895 m above mean sea level. The lake is roughly oval in shape with a north–south major axis (33 km long, 18 km wide) and has a surface area of 500 km^2. The land portion of the watershed has an area of 800 km^2. Lake Tahoe is considered a deep lake, with an average depth of 330 m, maximum depth of 501 m, and a total volume of 156 cubic km (it is the 11th deepest lake in the world). The surface layer of Lake Tahoe deepens during the fall and winter. Complete vertical mixing only occurs every few years. Due to its large thermal mass, Lake Tahoe does not freeze in winter. There are approximately 63 streams/rivers flowing into Lake Tahoe and only one river flowing out of Lake Tahoe to Pyramid Lake to the north and east of Lake Tahoe.

The Lake Tahoe automated validation site was established in 1999 to help validate the thermal infrared data and products from the Advanced Spaceborne Thermal Emission and Reflectance Radiometer (ASTER) and Moderate Resolution Imaging Spectroradiometer (MODIS) instruments on the Terra spacecraft launched in 1999 [23], [30]. Work at the site is performed by the University of California, Davis (UCD) and the Jet Propulsion Laboratory (JPL). A detailed description of the site is given by Hook *et al.* [10] and summarized here for completeness. Measurements at the site are made from four permanently moored buoys on the lake referred to as TB1, TB2, TB3, and TB4 and the U.S. Coast Guard (USCG) station

TABLE II
LATITUDE AND LONGITUDE POSITION OF THE LAKE TAHOE BUOYS. NOTE THE TWO SOUTHERN BUOYS WERE MOVED SLIGHTLY SOUTH IN LATE OCTOBER AND EARLY NOVEMBER 2002. LOCATIONS ARE GIVEN FOR THE BUOYS BEFORE AND AFTER THEY WERE MOVED

Buoy	05-07-1999 to present	06-16-1999 to present	05-07-1999 to 11-01-2002	11-01-2002 to present	06-16-1999 to 10-31-2002	10-31-2002 to present
TB1	39° 09.180 N 120° 00.020 W					
TB2			39° 08.292 N 120° 00.018 W	39° 06.562 N 120° 00.645 W		
TB3					39° 08.300 N 120° 04.920 W	39° 06.612 N 120° 04.521 W
TB4		39° 09.300 N 120° 04.330 W				

TABLE III
SPECIFICATIONS OF THE NIST-TRACEABLE STIRRED WATER BATH BLACKBODY USED TO CALIBRATE THE JPL RADIOMETERS AND THE TEMPERATURE-CONTROLLED WATER BATH WITH NIST-TRACEABLE THERMOMETER USED TO CALIBRATE THE SENSORS USED TO MEASURE THE BULK WATER TEMPERATURE. AN ADDITIONAL SECONDARY TEMPERATURE PROBE IS USED PERIODICALLY TO CROSS-CHECK THE CALIBRATION OF THE PRIMARY TEMPERATURE PROBE

Component	Accuracy	Stability	Precision
NIST designed cone in a 44 liter temperature controlled bath (Model 7008-IR)		at 25° C: +/- 0.0007° C	
Thermistor standard probe (Model 5643-R)	0.0015 ° C over 0-60 ° C	0.005 ° C / yr	
Readout system (Chub E4)	0.0025 ° C at 25 ° C		0.0001 ° C

located on the northwest shore of the lake (Table II). TB2 and TB3 were moved slightly farther south during the monitoring period, and Table II gives the positions before and after the move. Each buoy has a custom-built radiometer that measures the skin temperature and several temperature sensors that measure the bulk water temperature. The radiometers were built by JPL, and two radiometer models have been deployed at the site [4]. The earlier model had an accuracy of ± 0.2 °C, and the later model has an accuracy of ± 0.1 °C. The radiometers are calibrated in the laboratory using a NIST-traceable stirred water bath blackbody (Table III). The accuracy of the JPL radiometers was independently verified in both the laboratory and in the field. The laboratory comparision involved comparing the JPL field portable blackbody and JPL radiometers against the NIST blackbody and NIST transfer radiometer [12], [22]. The field comparison involved a cross comparison of several highly accurate radiometers, including the Marine Atmospheric Emitted Radiation Interferometer (MAERI), on a two-day cruise on the Research Vessel F. G. Walton Smith [4]. The results indicate the MAERI and JPL radiometers agreed to better than 0.1 °C. The bulk temperature measurements are made by several different temperature sensors mounted $\sim$2 cm beneath the surface on a floating support tethered behind each buoy. Four different types of bulk temperature sensor have been deployed at Lake Tahoe. These are the Optic Stowaway, Hobo Water Pro, Hobo Pro temp/external temp, and the MBLTA sensors. The four types of sensors have accuracies/resolutions of ± 0.25 °C/8-bit, ± 0.20 °C/12-bit, ± 0.20 °C/12-bit, and ± 0.10 °C/12-bit, respectively. The MBLTA sensors are manufactured by Apprise Technologies, and all the other sensors are manufactured by the Onset Corporation. The accuracies/resolutions are from the manufacturer's specification prior to recalibration at the JPL facility. The temperature sensors are recalibrated at JPL using a temperature-controlled water bath with an NIST-traceable thermometer (Table III). After recalibration, the 12-bit sensors are accurate to ± 0.1 °C. During the monitoring period, meteorological stations were added to each buoy. The meteorological measurements include wind speed, wind direction, relative humidity, air temperature atmospheric pressure, and net radiation. A full set of measurements (meteorology, bulk, and skin temperatures) are made every 2 min and stored on data loggers, which are read out either daily via telephone modem or every few months during site visits.

Both NASA/JPL and UCD maintain additional equipment at the U.S. Coast Guard Station. This includes a full meteorological station (wind speed, wind direction, relative humidity, air temperature, and atmospheric pressure), full radiation station (long and shortwave radiation up and down), a shadow band radiometer, and an all-sky camera. The shadow band radiometer provides information on total water vapor and aerosol optical depth. UCD also maintains two additional floats (rafts) in the southern part of Lake Tahoe that measure meteorological variables and bulk temperature.

Measurements of algal growth rate using 14C, nutrients (N, P), chlorophyll, phytoplankton, zooplankton, light, temperature, and secchi disk transparency are made from the UCD Research Vessel La Conte approximately biweekly, and many samples are taken annually around the Tahoe Basin for stream chemistry and snow constituents.

III. METHODOLOGY AND DATA PROCESSING

Several steps are involved in calculating the vicarious at-sensor radiance (predicted radiance) from the field data and then comparing that radiance with the satellite at-sensor radiance derived with the On Board Calibrator (OBC). These steps include the following:

- Step 1) extraction of the surface skin temperature from the field data;
- Step 2) forward propagation of the skin temperature to the at-sensor radiance using a radiative transfer model;
- Step 3) convolution of the at-sensor radiance with the Landsat system response function to obtain the vicarious at-sensor radiance for the Landsat band;
- Step 4) extraction of the at-sensor radiance from the Landsat data;
- Step 5) comparison of the vicarious and OBC at-sensor radiances.

The first three steps are described in Section III-A, and the last two steps are described in Section III-B. An error analysis for the derivation of the vicarious at-sensor radiance is provided under the Field Data Processing and Uncertainty Analysis section.

A. Field Data Processing and Uncertainty Analysis

The bulk water temperatures were extracted for each buoy at the time of the overpass from the multiple temperature sensors placed $\sim$2 cm beneath the surface at each buoy. Initially, the temperature trace of each sensor was examined and cross-compared with the other sensors on the same buoy to check all sensors were reading correctly. For a given bulk temperature sensor, the temperature at the time of the overpass was obtained by linearly interpolating between the two data points either side of the

overpass time to the overpass time. The average and standard deviation of the interpolated bulk temperature sensor values was then calculated for each buoy at the overpass time.

In order to compare the radiometer measurements to the satellite radiometric measurements, it is necessary to correct the field measurements to surface kinetic or skin temperature so they can be propagated through the atmosphere using the MODTRAN 3.5 RTC [5]. Once propagated, the top-of-atmospheric radiance is convolved to the L5B6 system response function and compared with the L5B6 radiance. The surface skin temperature is required, since the field radiometers measure the radiometric temperature over a different wavelength range than the satellite radiometers. In order to obtain the surface skin temperature, the radiometer data must be corrected for the reflected downwelling radiation from the atmosphere and the nonunit emissivity of the water. For a given wavelength interval, correction for the downwelling sky radiance reflected by the surface into the path of the radiometer is summarized as follows:

$$L_{\text{sur}} = \frac{L_{\text{obs}} - L_{\text{path}} - \tau(1-\varepsilon)L_{\text{down}}}{\tau\varepsilon} \tag{1}$$

where

L_{sur} surface radiance;
L_{obs} observed radiance;
L_{path} path radiance;
τ atmospheric transmission;
ε surface emissivity;
L_{down} downwelling atmospheric radiance.

Equation (1) is for a discrete wavelength interval, and the skin temperature is then obtained from the surface radiance by inverting the Planck equation. The radiance terms are calculated by integrating over the system response curve for the JPL self-calibrating radiometer

$$L_\lambda = \int_\lambda L(\lambda)R(\lambda)\partial\lambda. \tag{2}$$

Equation (2) is solved iteratively. The sky radiance term is obtained from the RTC driven by an atmospheric profile. The atmospheric profile is obtained from the National Center for Environmental Prediction (NCEP). The NCEP produces global model values on a $1^\circ \times 1^\circ$ grid at 6-h intervals. Lake Tahoe is centered on 39 N, 120 W, and the grid value for this point was utilized. The NCEP data were interpolated to the overpass time. The emissivity of the water was obtained from the ASTER spectral library available from http://speclib.jpl.nasa.gov.

In some cases, the skin temperature was not available at *any* station for a given overpass or for a particular station on a given overpass. If no skin temperatures were available for *any* stations for a given overpass, the average skin effect (bulk minus skin temperature) for *all* overpasses was subtracted from the average bulk temperature at each station to obtain the station skin temperature. If skin temperatures were available at some stations, but not all stations for a given overpass, then the average skin effect (bulk minus skin temperature) for *that* overpass was calculated and subtracted from the bulk temperatures to obtain the skin temperatures for the stations without a working radiometer. The bulk and skin temperatures are available from the author on request. There were 115 matchups (a matchup is where there is an *in situ* value and corresponding satellite value). Of these 115 matchups, only 82 were used in the analysis. Thirty-three matchups were excluded because the standard deviation of the bulk temperature sensors at the matchup was greater the 0.2 °C (see Section IV). Of the 82 matchups used, half were obtained using bulk temperature data with an assumed skin effect, and the other half were directly measured with a radiometer. Of the 24 validation days that were selected, eight utilized skin temperature estimates based on the average skin effect. All the other days used skin temperatures measured only by radiometers or measured by radiometers and bulk-derived skin temperatures where the skin effect was taken as the average skin effect from the other buoys with working radiometers at the overpass time.

TABLE IV
CHANGE IN THE CALCULATED AT-SENSOR L5B6 RADIANCE AND AT-SENSOR L5B6 BRIGHTNESS TEMPERATURE FOR VARIOUS PERTURBATIONS OF THE U.S. STANDARD ATMOSPHERIC MODEL FOR A GIVEN INPUT RADIANCE FOR A SITE AT THE ELEVATION OF LAKE TAHOE (~2 km)

Change from Nominal in Radiance (Brightness Temperature in brackets)	Adjusted radiance ($W/m^2.sr.\mu m$)	Radiance Difference ($W/m2.sr.\mu m$)	% Radiance Difference	Temperature Difference (°C)
90% Water Vapor	8.149	0.016	0.20%	0.13
110% Water Vapor	8.117	-0.016	-0.20%	-0.13
-1 deg C	8.127	-0.006	-0.07%	-0.05
+1 deg C	8.139	0.006	0.07%	0.05
50% Ozone	8.134	0.001	0.01%	0.01
150% Ozone	8.132	-0.001	-0.01%	0.01
50% Visibility (11.5 km)	8.104	-0.029	-0.36%	-0.24
150% Visibility (34.5 km)	8.143	0.01	0.12%	0.08

The nominal or original radiance was 8.133 $W/m^2.sr.\mu m$

The skin temperatures were then propagated to at-sensor radiance using the same RTC code and profile used to correct the radiometric data to skin temperature and the at-sensor radiance convolved with the L5B6 system response function to obtain an equivalent or vicarious Landsat radiance.

The need to correct the radiometric temperature to skin temperature with a downwelling radiance derived from the NCEP data introduces an uncertainty in the skin temperature. This uncertainty is very small (< 0.02 °C) and is discussed more fully in Hook *et al.* [10].

The skin temperature is propagated to the equivalent radiance at-sensor using an RTC. In the propagation to at-sensor radiance, the atmospheric path length is now the distance from the skin to the satellite as opposed to the distance from the radiometer to the skin, used to correct the radiometer temperature to skin temperature, and therefore the uncertainty is larger. Further, the size of this uncertainty is dependant on the spectral width of the band that the at-sensor radiance is convolved with, in this case L5B6. In other words, the size of the error associated with the forward prediction of the radiance for a given wavelength interval depends on where that interval is located in the thermal infrared region. Table IV shows the results from an assessment of the uncertainty associated with propagating the skin temperature to the satellite for a U.S. Standard Atmosphere. A U.S. Standard Atmosphere contains more water vapor than is typically encountered at Lake Tahoe, and therefore, the reported uncertainties represent the maximum uncertainty. The assessment involves modifying the various profile inputs and then calculating the difference between using the actual profile and the

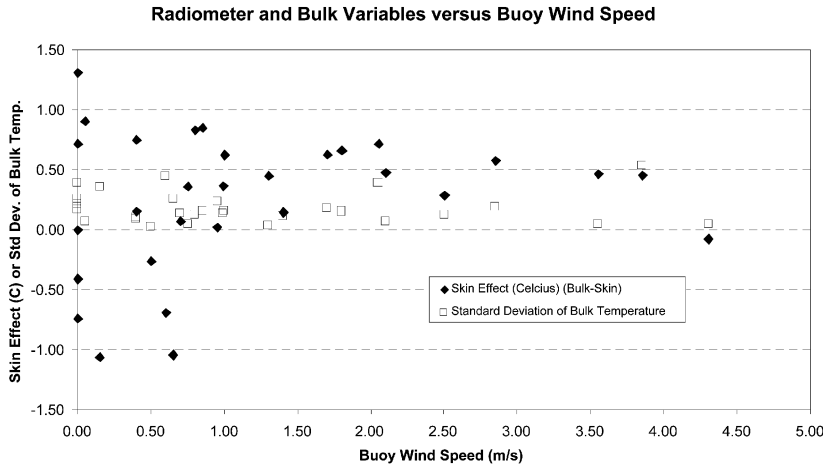

Fig. 1. Plot of skin effect (bulk temperature minus skin temperature) and standard deviation of bulk temperature sensors versus wind speed measured at Lake Tahoe buoys.

modified profile. This approach assesses the consequences of an error in the profile used to forward model the skin temperature to at-sensor radiance. For example, if the temperature profile is assumed to be in error by 1 °C, then 1 °C can be added to the profile, and the difference between forward propagated radiance using the nominal and adjusted profiles calculated similarly 1 °C can be subtracted from the profile and the difference between the forward propagated radiance using the nominal and adjusted profile calculated. It can be seen from Table IV that an error of 1 °C has a small effect on the difference between the brightness temperature obtained from the modified and unmodified profiles. The error associated with increasing the total water vapor in the profile by 10% is larger (0.13 °C) but still small. Clearly, the difference in the at-sensor radiance is most strongly related to the total water vapor in the profile, and therefore, sites with little water vapor in the overlying atmosphere, such as Lake Tahoe site, are highly desirable for validating the at-sensor radiance. The total column water vapor on clear days at Lake Tahoe is typically between 0.5–1.5 cm.

B. Landsat Image Data Processing

In order to select images suitable for validation, the L5 browse images acquired over Lake Tahoe from mid-1999 through 2003 were evaluated for cloud cover. Any images containing visible clouds over the lake were excluded, and the remaining images were purchased for further evaluation. The full-resolution visible and thermal infrared data were then examined, and any scenes with clouds over the lake that were not identified in the reduced spatial resolution browse, or could only be identified in the thermal infrared data, were excluded, resulting in 28 scenes that were suitable for validation. (Four of the 28 scenes were subsequently removed; see Section IV.) Comparison with ground data indicated these images spanned the full temperature range of the lake surface at the overpass time (~ 4 °C to -22 °C).

The TM sensor incorporates an onboard radiometric calibration system called the Internal Calibrator (IC), which is located in front of the primary focal plane. The IC consists of three silicon-detector-stabilized tungsten miniature lamps, a blackbody, and a shutter. Reflective bands use the lamps, and the thermal band uses the blackbody source for radiometric calibration. TM's thermal band calibration is achieved by periodic, once-per-scan viewing of the temperature-controlled blackbody source and the instrument shutter. At the end of each scan, the shutter on the calibrator arm swings in front of the detectors. This prevents detection of earth surface radiance in the calibration interval. During this period, the detectors sequentially view the calibration shutter and the blackbody whose temperatures are both known. The blackbody calibrator is controlled at a constant temperature throughout the instrument's lifetime, while the shutter temperature is uncontrolled, but monitored. Using the temperature-controlled blackbody source and shutter, a two-point calibration can be performed for the four thermal band detectors [1]. The response is quantized into eight-bit numbers that represent radiance values between 0–255.

The eight-bit instrument data were converted to radiance by applying the calibration coefficients supplied with the data. The application of the calibration coefficients to the instrument data to obtain the at-sensor radiance was confirmed using the raw image data, blackbody, and shutter information.

IV. Results and Discussion

A. Landsat Calibration

The measurements made at the buoys include both skin temperature and bulk temperature measured by the radiometers and the *in situ* temperature sensors, respectively. The skin temperature measurement is propagated through the atmosphere to obtain the equivalent radiance at sensor used for the forward calculation rather than the bulk temperature, since the satellite measures the skin temperature. Fig. 1 shows a plot of the standard deviation of the bulk temperature sensors and the skin effect (bulk minus skin temperature) versus the wind speed measured at the buoys. This plot only shows results for clear-sky overpasses where the skin and bulk temperatures and wind speed were measured simultaneously. Previous work by Hook *et al.* [10] utilized wind speeds measured at the USCG station on the northwest shore, which while providing a good indication of the general conditions, is not ideal, since wind speeds onshore can differ from wind speeds at the buoys, especially under light wind conditions. If the wind speed is low and the sky is clear, a strong diurnal cycle develops accompanied by stratification of the surface layer. Examination of Fig. 1 indicates that once the wind speed drops below 1 m/s, there is a wide range in the skin

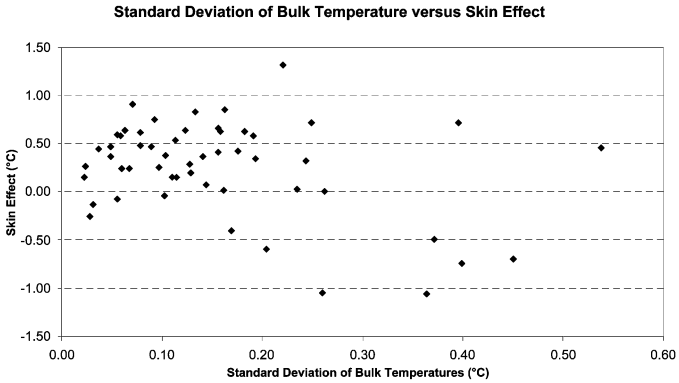

Fig. 2. Plot of skin effect (bulk temperature minus skin temperature) versus standard deviation of bulk temperature sensors measured at Lake Tahoe buoys.

effect, and the standard deviation of the bulk temperature sensors increases due to increased variability in the surface layer. This relationship is more apparent when the standard deviation of the bulk temperature sensors is plotted against the skin effect (Fig. 2). Examination of Fig. 2 indicates that when the standard deviation of the bulk temperature sensors is below 0.20 °C, the skin effect clusters around 0.5 °C, but when the standard deviation is greater than 0.20 °, the skin effect becomes quite variable ranging from −1.0 °C to 1.0 °C. As noted earlier, when no radiometer data are available at a buoy, an average skin effect is assumed; since, the skin effect is quite variable at the local scale, it was decided to only use data where the standard deviation of the bulk temperature measurements was ≤ 0.20 °C when the skin is homogenous, and the skin effect is reasonably constant. The observation that the skin effect remains relatively constant at higher wind speeds has also been noted for the oceans [7], although, Donlon observed a constant skin effect of 0.17 ± 0.07 K when the wind speed exceeded 6 m/s. The average skin effect, calculated for the Lake Tahoe scenes where the standard deviation of the bulk temperature values was $\leq$ 0.2 °C, was 0.35 ± 0.33°C. The larger skin effect and greater scatter in the skin effect in the Lake Tahoe data compared to the Donlon data are likely due to the inclusion of lower winds speeds. The skin effect at Lake Tahoe falls within the nominal range for the skin effect observed over the oceans [6], [9], [13], [14], [19], [27], [32]. The average skin effect observed at the Landsat overpass time is slightly larger than the average skin effect observed for the Terra overpass (ASTER and MODIS instruments), since the Landsat overpass is slightly earlier when the skin is cooler due to less solar heating. The Landsat overpass times used in this study range from 18:11 to 18:19 GMT. If all the skin effect data are used to calculate the average skin effect at the Landsat overpass time, including values when the standard deviation of the bulk temperature sensors was $>$ 0.20 °C, the average skin effect is 0.26 °C. This lower value reflects the fact that at lower wind speeds or higher bulk temperature standard deviations, the skin is often warmer than the bulk temperature leading to a negative skin effect (bulk minus skin temperature). Surface heterogeneity associated with the skin effect can be largely avoided if nighttime satellite data are used, but data from the Landsat instruments are not normally acquired at night.

Fig. 3 shows a plot of the vicarious at-sensor radiance (derived from the *in situ* data) versus the OBC at-sensor radiance. Again, only data where the standard deviation of the bulk temperature sensors was ≤ 0.20 °C are presented. Also, the average of the four potential values (one per buoy) for a given overpass is shown, unless there was only a single value for the overpass, in which case that value was excluded from the dataset. After this additional filtering, there were data from 24 of the original 28 overpass days, and these were used in the remainder of the study. Fig. 3 clearly shows the radiance underestimate and indicates there is a bias between the OBC radiance and vicarious radiance. The average radiance bias is 1.54% (1.0 °C), which compares to an average bias calculated by Barsi *et al.* [1] of 0.7 °C. If the difference between the vicarious and OBC radiance is plotted against time, the size of the error changes with time (Fig. 4). In Fig. 4, the bias starts off at 2.5% (1.6 °C) in late 1999 and then gradually decreases to 0.8% (0.5 °C) in mid-2002. From mid-2002 to the present, the bias fluctuates between 0.3% (0.2 °C) and 1.4% (0.9 °C). The cause of this bias is unresolved but is likely due to a decrease in the performance of the instrument coupled with changes in the temperature of the instrument. The instrument has undergone large changes in temperature in recent years, since many of the ground stations have stopping receiving Landsat-5 data and starting receiving Landsat-7 ETM+ data instead.

B. Surface Temperature Recovery

The radiance received by an earth-orbiting sensor in the thermal infrared (7–13 μm) part of the electromagnetic spectrum consists of a surface and atmospheric component. The surface component depends on the temperature and emissivity of the surface, and the atmospheric component depends on the temperature and composition of the atmosphere, primarily the amount of water vapor present. Instruments designed to recover SST like the AVHRR and the ATSR typically place one band in the clearest part (least sensitive to water vapor) of the thermal infrared spectrum and the other band in a different part of the thermal infrared spectrum that is sensitive to water vapor. If the emissivity of water in each of the bands is assumed to be constant, the at-sensor radiance sensed by the two bands varies based on the temperature of the surface and the amount of water vapor in the atmosphere. As a result, the at-sensor radiance data from the two bands can be regressed to surface measurements to obtain coefficients for recovering the water temperature that account for the variation in the water vapor in the atmosphere. Since the Landsat TM instrument only has a single band in the thermal infrared part of the electromagnetic spectrum (L5B6), this same regression approach cannot be used unless additional information on the composition of the atmosphere is supplied. The Landsat TM instrument only has a single broad thermal infrared band in order to be able to acquire data at much higher spatial resolutions with the equivalent signal to noise as the AVHRR and the ATSR instruments. AVHRR and ATSR have spatial resolutions of $\sim$1 km at nadir compared to 120 and 60 m for Landsat-5 TM and Landsat ETM+, respectively. Although Landsat does not have two bands to account for water vapor, a surrogate value can be obtained from the total column water vapor available with the NCEP data. The NCEP data are the same data used to forward model the ground temperatures to at-sensor radiance described previously. Total Column Water could also be derived from the Multi Filter Rotating Shadowband Radiometer data acquired at the site; however, these

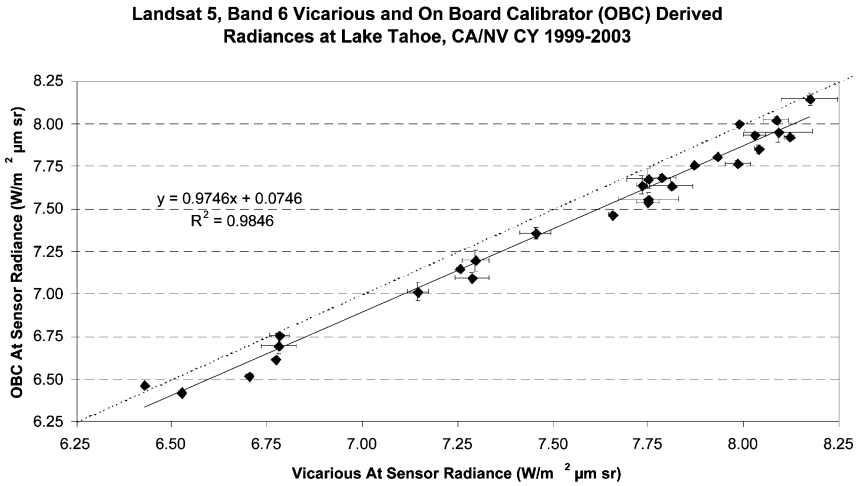

Fig. 3. Plot of L5B6 OBC radiance versus L5B6 vicarious (predicted) radiances. X error bars are the standard deviation of the vicarious at sensor radiance for each overpass. Y error bars are the standard deviation of the OBC at sensor radiance for each overpass.

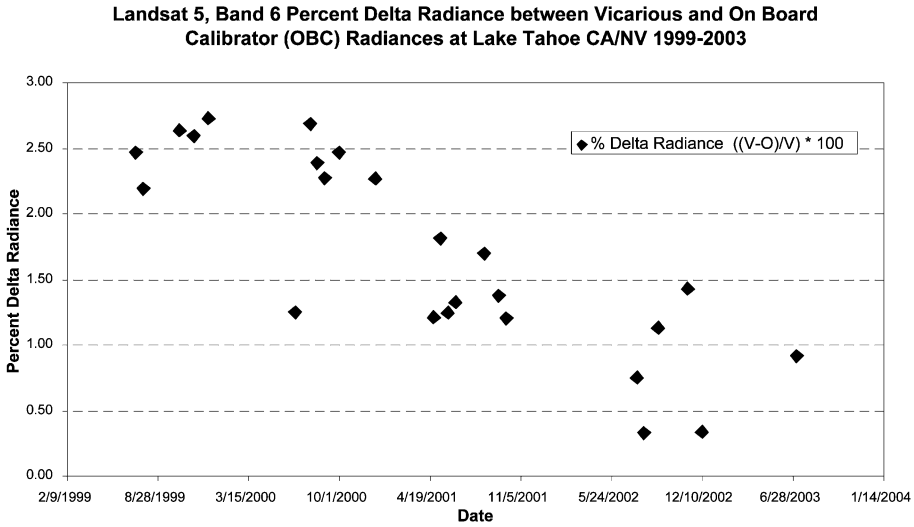

Fig. 4. Plot of the percent radiance difference between the vicarious (V) and OBC at-sensor radiances over time. Percent radiance differences calculated at $(\mathrm{V}-\mathrm{O})/\mathrm{V}*100$.

data were not used, since they were not available for all the overpasses.

Table V shows the coefficients and fit values from regressing various combinations of the L5B6 radiances, NCEP values, and vicarious radiances to the skin and bulk temperatures. Evaluation of this table indicates that the smallest error is obtained if the forward propagated skin temperature values are regressed back to themselves (standard error of regression or S.E. $= 0.239$ °C). Note that no L5 data are used in this regression. This error is a direct measure of the best possible result that could be obtained from a perfect measure of the satellite radiance. It is only slightly better than the error calculated by Hook *et al.* [10] from ATSR2 data (S.E. $= 0.33$ °C). The worst error is obtained from a simple fit of the L5B6 values to the skin temperatures (S.E. $= 0.67$ °C). Again, this is expected, since the single-band value does not provide any means to account for variability in the atmospheric water vapor as discussed earlier. Slightly better standard errors are obtained when the L5B6 and NCEP data are regressed to either the skin or the bulk temperatures (0.63 °C and 0.62 °C for regressions to the skin and bulk temperature, respectively). The fact that the regressions give similar results for both the skin and the bulk temperatures suggests that the skin effect is relatively constant as expected based on the filtering of the scenes to only those where the standard deviation of the bulk temperatures was ≤ 0.20 °C. Since the L5B6 data were regressed to *in situ* data, the regression accounts for an average bias observed in the in-flight validation; however, they do not account for random instrument noise, which explains why the S.E. for the data is not as good as that observed with ATSR2 data. The coefficients presented in Table V could be used by other investigators to derive skin or bulk temperatures from L5B6 data, for similar areas, i.e., high-altitude lakes with relatively dry atmospheres. Further analyses are required to confirm that this approach works correctly with wetter atmospheres.

V. Summary and Conclusion

The absolute calibration of the Landsat-5 TM thermal infrared band (L5B6) was assessed from mid–1999 through 2003 using

TABLE V
LINEAR COEFFICIENTS DERIVED FROM REGRESSION OF THE VICARIOUS L5B6 RADIANCES, OBC L5B6 RADIANCES, AND NCEP TOTAL COLUMN WATER VAPOR AGAINST THE SURFACE SKIN TEMPERATURE AND BULK TEMPERATURE FOR THE FOUR BUOYS AT THE TIME OF THE LANDSAT-5 OVERPASS. L5ASR = L5 AT-SENSOR RADIANCE. TCW = TOTAL COLUMN WATER VASR = VICARIOUS AT-SENSOR RADIANCE. X1 AND X2 REFER TO THE COEFFICIENT THAT THE INPUT DATA SHOULD BE MULTIPLIED BY IN ORDER TO OBTAIN THE Y VARIABLE. FOR EXAMPLE TO DERIVE THE SKIN TEMPERATURE FROM THE LANDSAT RADIANCE (L5ASR), USING JUST LANDSAT DATA, THE L5ASR IS MULTIPLIED BY, X1 AND THE INTERCEPT IS ADDED. TO DERIVE THE SKIN TEMPERATURE FROM THE LANDSAT RADIANCE (L5ASR) AND TOTAL COLUMN WATER (TCW), THE L5ASR IS MULTIPLIED BY X1, AND THE TCW IS MULTIPLIED BY X2. THE PRODUCTS ARE SUMMED, AND THE INTERCEPT IS ADDED

Y Variable	X Variables	Intercept	X1	X2	N	R^2	Standard Error of Regression
Daytime Skin	L5C6	-53.034	9.118		82	0.978	0.674
Daytime Skin	L5ASR and TCW	-51.924	0.683	8.886	82	0.981	0.633
Daytime Bulk	L5ASR and TCW	-51.403	0.412	8.894	82	0.982	0.616
Daytime Skin	VASR and TCW (No L5 data)	-52.027	8.707	1.033	82	0.997	0.239
Daytime Bulk	VASR and TCW (No L5 data)	-51.335	8.691	0.774	82	0.994	0.357

water skin and bulk temperature data from an automated validation site at Lake Tahoe. The bulk and skin temperature data are acquired every 2 min from four permanently moored buoys on the lake. Assessment involved taking the skin temperature at the time of the overpass and predicting the at-sensor radiance with a RTC. The at-sensor radiance was then convolved with the L5B6 system response function and compared with the radiance measured by L5B6. Twenty-four cloud free scenes were used in the assessment with ground temperature ranging between $4\,^{\circ}$C and $22\,^{\circ}$C. The skin temperatures used in the forward propagation were on average $0.34\,^{\circ}$C cooler than the bulk temperatures. Results indicate that L5B6 had a bias of 2.5% ($1.6\,^{\circ}$C) in late 1999 that gradually decreased to 0.8% ($0.5\,^{\circ}$C) in mid-2002. From mid-2002 to the present, the bias fluctuates between 0.3% ($0.2\,^{\circ}$C) and 1.4% ($0.9\,^{\circ}$C). The exact cause for this bias is unresolved but is likely related to changes in the instrument temperature associated with changes in instrument usage.

The *in situ* data used to validate the instrument were also used to develop an approach for recovering the skin and bulk temperature of water. The approach involved regression of the at-sensor radiance data together with an estimate of the total column water vapor from NECP data with the *in situ* measurements of skin and bulk water temperature. The standard errors for the regression were $0.63\,^{\circ}$C and $0.62\,^{\circ}$C for the recovery of the skin and bulk water temperatures, respectively. These errors set a limit on the recovery of water temperature with L5B6 data. Although these errors are slightly larger than those obtained from instruments with two bands in the thermal infrared such as ATSR2, the skin and bulk temperatures can be derived a far higher spatial resolutions, making them more useful for research involving small water bodies such as small lakes and rivers. The coefficients developed with the regression are for high-altitude lakes with relative dry atmospheres above them. Further work is required to determine if these coefficients need to be adjusted for use with warmer lakes with wetter atmospheres.

It is remarkable that the Landsat-5 TM has continued to perform so well for a time period far exceeding its original design life. Nevertheless, the instrument has aged, and its characteristics have changed since its launch. These changes must be adequately characterized and corrected to preserve the usefulness of the acquired data. These results demonstrate the need for calibration of an instrument over its lifetime as well shortly after launch in order to assess the true radiometric response of an instrument as accurately as possible.

ACKNOWLEDGMENT

Numerous people have contributed to this work. In particular, the authors would like to thank the UCD Tahoe Research Group and W. Boncyk (Ball Aerospace and Technologies Corporation, now at JPL) for providing numerous helpful suggestions.

REFERENCES

[1] J. A. Barsi, J. R. Schott, F. D. Palluconi, D. L. Helder, S. J. Hook, B. L. Markham, G. Chander, and E. M. O'Donnell, "Landsat TM and ETM+ thermal band calibration," *Can. J. Remote Sens.*, vol. 29, pp. 141–153, 2003.

[2] J. A. Barsi, J. L. Barker, and J. R. Schott, "An atmospheric correction parameter calculator for a single thermal band earth-sensing instrument," in *Proc. IGARSS*, Toulouse, France, July 21–25, 2003.

[3] I. J. Barton, "Satellite-derived sea-surface temperatures—Current status," *J. Geophys. Res.—Oceans*, vol. 100, pp. 8777–8790, 1995.

[4] I. J. Barton, P. J. Minnett, K. A. Maillet, C. J. Donlon, S. J. Hook, A. T. Jessup, and T. J. Nightingale, "The Miami2001 infrared radiometer calibration and inter-comparison: Ship comparisons," *J. Atmos. Oceanic Technol.*, vol. 21, pp. 268–283, 2004.

[5] A. Berk, L. S. Bernstein, and D. C. Robertson, "MODTRAN: A moderate resolution model for LOWTRAN 7," Geophys. Lab., Bedford, MA, Tech. Rep. GL-TR-89-0122, 1989.

[6] C. J. Donlon and I. S. Robinson, "Radiometric validation of ERS-1 along track scanning radiometer average sea surface temperature in the Atlantic Ocean," *J. Atmos. Oceanic Technol.*, vol. 15, pp. 647–660, 1998.

[7] C. J. Donlon, "Implications of the oceanic SST deviation at high wind speed," *Geophys. Res. Lett.*, vol. 26, pp. 2505–2508, 1999.

[8] C. J. Donlon, P. J. Minnett, C. Gentemann, T. J. Nightingale, I. J. Barton, B. Ward, and M. J. Murray, "Toward improved validation of satellite sea surface skin temperature measurements for climate research," *J. Clim.*, vol. 15, pp. 353–369, 2002.

[9] C. W. Fairall, E. F. Bradley, J. S. Godfrey, G. A. Wick, J. B. Edson, and G. S. Young, "Cool-skin and warm-layer effects on sea surface temperature," *J. Geophys. Res.—Oceans*, vol. 101, pp. 1295–1308, 1996.

[10] S. J. Hook, A. J. Prata, R. E. Alley, A. Abtahi, R. C. Richards, S. G. Schladow, and S. Ó. Pálmarsson, "Retrieval of lake bulk and skin temperatures using Along-Track Scanning Radiometer (ATSR-2) data: A case study using Lake Tahoe, California," *J. Atmos. Oceanic Technol.*, vol. 20, pp. 534–548, 2003.

[11] J. Imberger and J. C. Patterson, "Physical limnology," *Adv. Appl. Mech.*, vol. 27, pp. 303–475, 1990.

[12] B. Kannenberg, "IR instrument comparison workshop at the Rosenstiel School of Marine and Atmospheric Science (RSMAS)," *Earth Obs.*, vol. 10, 1998.

[13] K. B. Katsaros, "Sea-surface temperature deviation at very low wind speeds—Is there a limit," *Tellus*, vol. 29, pp. 229–239, 1997.

[14] K. B. Katsaros, W. T. Liu, J. A. Businger, and J. E. Tillman, "Heat-transport and thermal structure in interfacial boundary-layer measured in an open tank of water in turbulent free convection," *J. Fluid Mech.*, vol. 83, p. 311, 1977.

[15] E. J. Kearns, J. A. Hanafin, R. H. Evans, P. J. Minnett, and O. B. Brown, "An independent assessment of pathfinder AVHRR sea surface temperature accuracy using the Marine Atmosphere Emitted Radiance Interferometer (MAERI)," *Bull. Amer. Meteorol. Soc.*, vol. 81, pp. 1525–1536, 2000.

[16] C. H. Mortimer, "Water movements in lakes during summer stratification; Evidence from the distribution of temperature in Windermere," *Phil. Trans. R. Soc. London*, vol. B236, pp. 355–404, 1952.

[17] S. G. Monismith, "Wind-forces motion in stratified lakes and their effect on mixed-layer shear," *Limnol. Oceanogr.*, vol. 30, pp. 771–783, 1985.

[18] ——, "An experimental study of the upwelling response of stratified reservoirs to surface shear stress," *J. Fluid Mech.*, vol. 171, pp. 407–439, 1986.

[19] M. J. Murray, M. R. Allen, C. J. Merchant, A. R. Harris, and C. J. Donlon, "Direct observation of the skin-bulk SST variability," *Geophys. Res. Lett.*, vol. 27, pp. 1171–1174, 2000.
[20] E. P. McClain, "Comparitive performance of AVHRR multiband SSTs," *J. Geophys. Res.*, vol. 90, pp. 11,587–11 601, 1985.
[21] E. M. O'Donnell, J. R. Schott, and N. G. Raqueno, "Calibration history of Landsat thermal data," in *Proc. IGARSS* , vol. 1, Toronto, ON, Canada, 2002, pp. 27–29.
[22] J. P. Rice, J. J. Butler, B. C. Johnson, P. J. Minnett, K. A. Maillet, T. J. Nightingale, S. J. Hook, A. Abtahi, C. J. Donlon, and I. J. Barton, "The Miami2001 infrared radiometer calibration and intercomparison. Part I: Laboratory characterization of blackbody targets," *J. Atmos. Oceanic Technol.*, vol. 21, pp. 258–267, 2004.
[23] V. V. Salomonson, W. L. Barnes, P. W. Maymon, H. E. Montgomery, and H. Ostrow, "MODIS: Advanced facility instrument for studies of the earth as a system," *IEEE Trans. Geosci. Remote Sensing*, vol. 27, pp. 145–153, Jan. 1989.
[24] P. Schluessel, H. Y. Shin, W. J. Emery, and H. Grassl, "Comparison of satellite-derived sea-surface temperatures with insitu skin measurements," *J. Geophys. Res.—Oceans*, vol. 92, pp. 2859–2874, 1987.
[25] J. R. Schott and W. J. Volchok, "Thematic Mapper thermal infrared calibration," *Photogramm. Eng. Remote Sens.*, vol. 51, pp. 1351–1357, 1985.
[26] J. R. Schott, "Thematic Mapper, band 6, radiometric calibration and assessment," *Proc. SPIE*, vol. 924, pp. 72–88, 1988.
[27] A. V. Soloviev and P. Schlussel, "Evolution of cool skin and direct air–sea gas transfer coefficient during daytime," *Bound.-Layer Meteorol.*, vol. 77, pp. 45–68, 1996.
[28] P. T. Strub and T. M. Powell, "Wind-driven surface transport in stratified closed basins: Direct versus residual calculation," *J. Geophys. Res.*, vol. 91, pp. 8497–8508, 1986.
[29] ——, "Surface temperature and transport in Lake Tahoe: Inferences from satellite (AVHRR) imagery," *Continent. Shelf Res.*, vol. 7, pp. 1001–1013, 1987.
[30] Y. Yamaguchi, A. B. Kahle, H. Tsu, T. Kawakami, and M. Pniel, "Overview of advanced spaceborne thermal emission reflectance radiometer," *IEEE Trans. Geosci. Remote Sensing*, vol. 36, pp. 1062–1071, July 1998.
[31] C. C. Walton, W. G. Pichel, J. F. Sapper, and D. A. May, "The development and operational application of nonlinear algorithms for the measurement of sea surface temperatures with the NOAA polar-orbiting environmental satellites," *J. Geophys. Res.—Oceans*, vol. 103, pp. 27 999–28012, 1998.
[32] G. A. Wick, W. J. Emery, L. H. Kantha, and P. Schlussel, "The behavior of the bulk-skin sea surface temperature difference under varying wind speed and heat flux," *J. Phys. Oceanogr.*, vol. 26, pp. 1969–1988, 1996.
[33] A. M. Zavody, C. T. Mutlow, and D. T. Llewellyn-Jones, "A radiative transfer model for SST retrieval for the ATSR," *J. Geophys. Res.*, vol. 100, pp. 937–952, 1995.

Simon J. Hook received the B.Sc. degree from the University of Durham, Durham, U.K., in 1982, the M.Sc. degree from the University of Alberta, Edmonton, AB, Canada, in 1985, and the Ph.D. degree from the University of Durham, in 1989, all in geology.

From 1989 to 1991, he was a National Research Council Resident Research Associate wih the National Aeronautics and Space Administration Jet Propulsion Laboratory (JPL), Pasadena, CA. Since 1991, he has been a Technical Staff Member at JPL. From 1993 to 2003, he was the Project Scientist for the Advanced Spaceborne Thermal Emission and Reflectance Radiometer (ASTER). In addition to his work on ASTER, he has been involved in the validation of several airborne and spaceborne instruments, including Landsat-5 and ETM+, the Moderate Resolution Imaging Spectroradiometer (MODIS), MASTER (the MODIS/ASTER Airborne Simulator), the European Along-Track Scanning Radiometers (ATSR2 and AATSR), and the DOE Multispectral Thermal Imager. His research is focused on the use of solar reflective and thermal infrared remotely sensed data in geology and ecology with a special emphasis on in-flight calibration and validation.

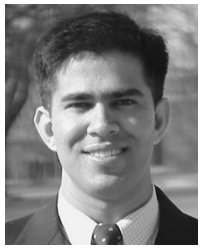

Gyanesh Chander received the M.S. degree in electrical engineering from South Dakota State University, Brookings, in 2001.

He is currently a Scientist with Science Applications International Corporation (SAIC) at the Earth Resources Observation System Data Center, U.S. Geological Survey, Sioux Falls, SD. He works on radiometric characterization and calibration of satellites and airborne instruments.

Julia A. Barsi received the B.S. and M.S. degrees in imaging science with a concentration in remote sensing from the Rochester Institute of Technology, Rochester, NY.

She is currently a Calibration Analyst with Science Systems and Applications, Incorporated, Greenbelt, MD. She is involved with the characterization and calibration of the Landsat sensors, with an emphasis on the thermal band calibration.

Ronald E. Alley, photograph and biography not available at the time of publication.

Ali Abtahi, photograph and biography not available at the time of publication.

Frank D. Palluconi is a member of the Jet Propulsion Laboratory, Pasadena, CA. His research interests are in thermal measurement instrumentation, atmospheric correction, and their application to the understanding of planetary surfaces and surface processes. He is an EOS ASTER Team Member, a Landsat-7 Calibration Team Member, and the Project Scientist for the Mars Science Laboratory 2009 Rover Mission.

Brian L. Markham (M'04) received the B.S. degree with a specialization in natural resources and the M.S. degree in remote sensing from Cornell University, Ithaca, NY, in 1976 and 1978, respectively, and the M.S. degree in applied physics from The Johns Hopkins University, Baltimore, MD, in 1996.

He has been a Physical Scientist at the National Aeronautics and Space Administration Goddard Space Flight Center, Greenbelt, MD, since 1978. His research has focused on characterizing the radiometric properties of ground, aircraft, and satellite sensor systems, as well as characterizing atmospheric aerosol optical properties for correction of optical remote sensing data. He has been the Landsat Calibration Scientist since 1993, where he has been involved in the prelaunch and on-orbit radiometric characterization and calibration of the Landsat-7 ETM+ sensor.

Robert C. Richards received the B.A. and M.A. degrees in zoology from the University of California, Davis (UC Davis) in 1961 and 1989, respectively.

He is currently a Research Limnologist with UC Davis. He has been a coauthor or lead author on over 27 research papers and has given oral presentations at international, national, and regional limnological meetings.

S. Geoffrey Schladow is a Professor of civil and environmental engineering at the University of California (UC Davis), Davis, and Director of the UC Davis Tahoe Environmental Research Center. His research interests include mixing and transport processes in aquatic systems, water quality modeling, and the linkages between fluid mechanics and the determinants of water quality and ecological well-being.

Dennis L. Helder (S'88–M'90) received the B.S. degrees in animal science and electrical engineering, the M.S. degree in electrical engineering from South Dakota State University, Brookings, and the Ph.D. degree in electrical engineering from North Dakota State University, Fargo, in 1979, 1980, 1985, and 1991, respectively.

For the past ten years, he has worked extensively with the Earth Resources Observation System Data Center, the National Aeronautics and Space Administration Goddard Space Flight Center (GSFC), and Stennis Space Center in the area of radiometric, geometric, and spatial calibration of satellite imagery. Other activities include consulting, membership on the international Committee of Earth Observation Satellites Infrared, Visible, and Optical Sensor's subcommittee, a Visiting Scientist appointment at GSFC, development of the Landsat-7 image assessment system with GSFC, and design of aircraft imaging systems.